11

Contrail Cirrus

ULRICH SCHUMANN

A contrail (a term introduced for "condensation trail" in 1942 by British pilots) is a visible cloud forming behind aircraft, mainly due to water vapor emissions from the engines. Contrails were first observed behind propeller-driven aircraft in 1915 but form as well from the exhaust of jet engines in cold ambient air (Schumann 1996a).

Contrails are visible indicators of cruising aircraft and may impact the Earth's climate. Aircraft exhaust may influence cloud formation either directly by forming contrails or indirectly by causing an aerosol of black carbon soot, volatile particles, and metallic particles which later impact the formation and properties of cirrus clouds in the same air mass at other places.

Though the cover by contrails is small compared to the cover by natural cirrus clouds, the potential climatic importance of contrails is being studied intensively. A review of the results obtained so far has been prepared for an assessment on *Aviation and the Global Atmosphere* (IPCC 1999). It reveals considerable progress in understanding aviation-produced aerosols and cloudiness (Fahey and Schumann 1999). Contrail studies also aid in learning about cirrus formation because contrails are cirrus clouds that form under relatively well defined and reproducible conditions. This chapter reviews some of the progress in understanding contrail formation, occurrence, properties, and radiative impact and identifies some important unanswered questions.

11.1. Contrail Formation

Contrail formation can be accurately predicted for given atmospheric temperature and humidity conditions. Contrails form thermodynamically according to the Schmidt-Appleman criterion (Schmidt 1941; Appleman 1953) when the relative humidity (RH) in the plume of exhaust gases mixing with ambient air temporarily reaches or exceeds liquid saturation, so that liquid droplets form on cloud-condensation nuclei (CCN) and soon freeze to ice particles. Measurements have shown that liquid saturation is indeed necessary (see fig. 11.1) and that contrails do not form when the RH exceeds ice saturation (Jensen et al. 1998b; Kärcher et al. 1998a; Schumann et al. 2000). The maximum RH reaches liquid saturation

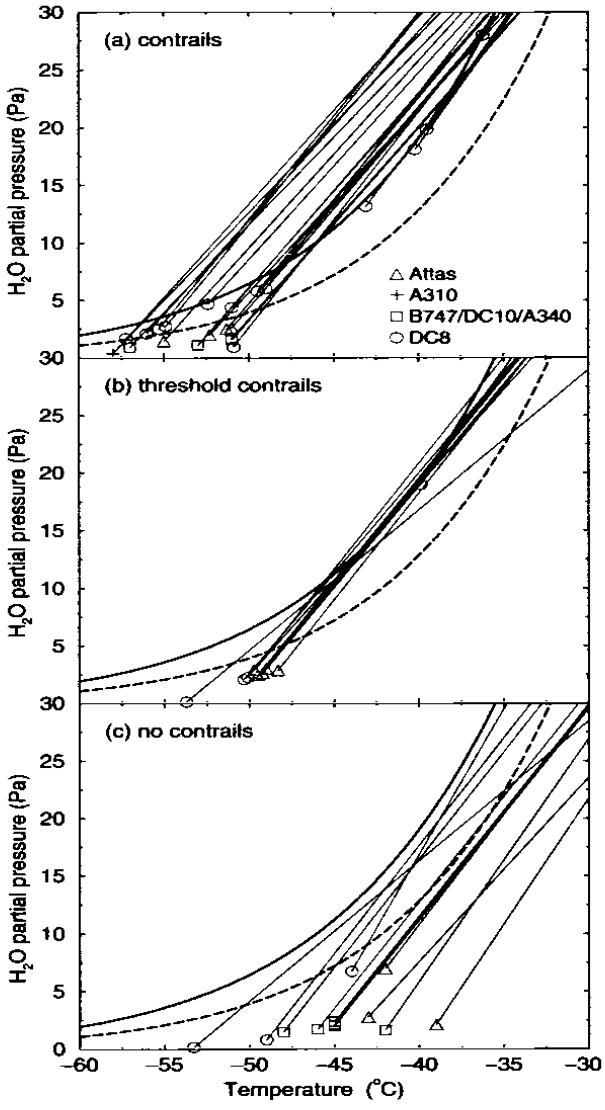

Figure 11.1. Observations indicating that contrails form when the mixing of exhaust gases with ambient air leads to liquid saturation. The data are grouped according to cases with (a) observed contrails (b) observed onset of contrail formation, and (c) no contrails. The symbols represent measured temperature and water vapor partial pressure of ambient air near cruising aircraft of known type. The lines departing from the point of ambient conditions represent the mixing lines with slopes depending on the parameters given in the text. The curves represent saturation pressure for liquid (full) and ice (dashed) saturation. From Kärcher et al. (1998a).

when the ambient temperature is below a threshold temperature of typically –50° to –35°C, depending on ambient pressure and humidity and aircraft properties. This maximum is reached in the young plume (age <0.5 s) closely behind the aircraft. In the aging plume, kilometers behind the aircraft, the relative humidity decreases and approaches the humidity of the ambient air. Persistent contrail formation requires that the ambient atmosphere is ice-saturated (Brewer 1946; Jensen et al. 1998b).

Aircraft exhaust may lead to cirrus clouds where no clouds would have formed otherwise. Ice-supersaturated air is often free of visible clouds because the supersaturation is too small for ice particle nucleation to occur (Heymsfield et al. 1998b; Gierens et al. 1999b). Persistent contrails may last for hours and grow into a spreading cirrus cloud. Although aircraft flying through ice-supersaturated air masses trigger contrail formation by the increase of humidity within their exhaust trails, the ice formed in long-lasting contrails originates almost completely from ambient water vapor (Knollenberg 1972).

The threshold temperature for contrail formation in the Schmidt-Appleman criterion depends on ambient pressure, p, and ambient RH and on the parameters that determine the steepness, $de/dT = \mathrm{EI_{H_2O}}\, c_p\, p/[0.622\, Q_{\mathrm{eff}}]$, of the mixing line (fig. 11.1) of excess partial water pressure, e, versus excess temperature, T, in the plume (Schumann 1996a). The parameters include the emission index (EI) of water mass per burnt fuel mass ($\mathrm{EI_{H_2O}} \cong 1.25$ for typical jet fuels with 13.8% hydrogen mass fraction), the specific heat capacity of air, $c_p \cong 1004\,\mathrm{J/kg\,K^{-1}}$, and the effective amount of heat, Q_{eff}, released into the exhaust per unit fuel mass, where $Q_{\mathrm{eff}} = (1 - \eta)\, Q$ depends on the specific heat of combustion of the fuel in the engine ($Q \cong 43\,\mathrm{MJ/kg}$) and the overall efficiency, η, of the aircraft propulsion system. The dependence on engine efficiency was noted by Schmidt (1941). The efficiency can be computed from $\eta = (F\,V)/(m_F\,Q)$ for given engine thrust, F, aircraft speed, V, engine fuel consumption rate, m_F, and Q (Schumann 1996a). Propulsion engineers call m_F/F the specific fuel consumption. Typical values of η are in the range 0.2–0.4, its value grew from older low-bypass to modern high-bypass engines. Some authors use "contrail factors" $\mathrm{EI_{H_2O}}/Q_{\mathrm{eff}}$ explicitly depending on the by-pass ratio of engines (Coleman 1996; Ferris 1996; Mazin 1996; Schrader 1997).

The spatial scales and the lifetime of contrails depend on ambient humidity and the rate of mixing, $(dN/dt)/N$. The dilution factor, N, measures the mass of air with which the exhaust from a unit mass of burnt fuel mixes. The mixing process depends on different mechanisms and proceeds at different rates in the early jet regime, the vortex regime, the vortex breakup regime, and the atmospheric dispersion regime (Gerz et al. 1998). The dispersion regime ends when the plume concentrations are diluted to ambient concentration levels within their natural range of variability. For modern large subsonic aircraft, the regimes typically extend to plume ages of 10 s, 100 s, 3 min, and 3 h, respectively. The dilution factor has been measured in a large set of field experiments (Schumann et al. 1998) and has been found to vary approximately with plume age, t, as $N = 7000\,(t/t_0)^{0.8}$, $t_0 = 1$ s, for t from 6 ms to 10^4 s.

The three-dimensional vortex dynamics and the mixing processes have been studied in large-eddy simulations (e.g., Lewellen and Lewellen 1996; Gerz et al.

1998), partly including cloud microphysical processes (Gierens 1996; Gierens and Jensen 1998; Jensen et al. 1998a). Details of the structure of contrails have been measured with Lidar methods (Freudenthaler et al. 1995; Sassen and Hsueh 1998; Sussmann 1999) and in situ techniques (Petzold et al. 1997; Ström and Ohlsson 1998b). At the end of the vortex regime, contrails are grown vertically to 150–300 m depth with little horizontal spreading. The vertical extent of contrails is smaller the more stable the stratification of the atmosphere. Horizontal growth in the dispersion regime is often dominated by wind shear that spreads a contrail to a band of several kilometers in width. Measured growth rates of width vary between 18 and 140 m/min and of cross-section between 3500 and 25,000 m^2/min. Contrails older than 15 min may extend more than 300–800 m vertical depth (Freudenthaler et al. 1995). The life cycle of contrails under the impact of complex atmospheric motions, evaporating and sedimenting particles, and radiative heat sources (Gierens and Jensen 1998; Jensen et al. 1998a) are still being investigated.

11.2. Particle Formation in Contrails

The formation of contrail particles is a complex microphysical process, which we understand today far better than a few years ago (Miake-Lye et al. 1993). The number of ice particles that are formed behind an aircraft depend on ambient humidity and temperature, on the amount of emitted ions, soot particles, sulfur content of the fuel, fraction of fuel sulfur oxidized to sulfuric acid, the rate of homogeneous and heterogeneous freezing of supercooled solutions, the efficiency of SO_2 heterogeneous oxidation, the effect of other condensable gases such as HNO_3, and ambient aerosols (Yu and Turco 1998a). Figure 11.1 implies that contrail particles form first as liquid droplets. Many of the liquid droplets must freeze quickly in the jet plume at ages less than 0.1 s because otherwise they cannot grow large enough to form a visible contrail some 10 m behind the engine as observed (Kärcher et al. 1996; Schumann 1996b). For droplet formation by water condensation, cloud condensation nuclei (CCN) must be available. Ambient aerosol contains too few CCNs to explain the large number of ice particles (10^4–10^5/cm) required for the early visibility of contrails 10–30 m behind engine exit (Kärcher 1996). In addition to entrained ambient aerosol, the CCN sources include soot particles and freshly nucleated sulfuric acid/water droplets (Kärcher et al. 1996), parts of which form on chemi-ions emitted by the engines (Yu and Turco 1998b).

The number of small particles in engine plumes has been measured with condensation-nucleus (CN) counters which count the number of particles grown in a saturated environment inside the instrument to optically detectable sizes. Such instruments detect particles larger than a threshold diameter of 3–20 nm. Using exhaust samples from heated or unheated inlets, the instruments determine the nonvolatile (soot) or total particle fractions. By reference to the excess concentration of conserved species such as CO_2 in the plume, one can determine the EI of particles (i.e., the number of particles emitted per unit mass of burnt fuel). Aerosol particle and ice crystal size distributions in the range of 150 nm to

500 μm have been measured by optical particle spectrometers, replicators, and by counterflow virtual impactors selecting ice particles larger than about 5 μm (Goodman et al. 1998; Lawson et al. 1998; Schröder et al. 2000). Soot size distributions have been determined by spectrometers for dry aerosols (Hagen et al. 1998; Petzold et al. 1999a; Pueschel et al. 1998). Detailed size spectra of aircraft-induced aerosol at diameters less than 150 nm are becoming available now from measurements with cascades of CN counters. Size spectra were previously measured by counting the particles in various size intervals discriminated by electrical aerosol-size qualifiers (Hagen et al. 1996). When analyzing such measured size spectra (e.g., Konopka et al. 1997), one must be aware of the drying process between sample inlet and particle counters. Previous measurements may overestimate the contribution from ambient particles larger than 300 nm (before drying) or from particles contained in ice particles larger than 300 nm because of anisokinetic sampling inlets.

So far, the measurements show that aircraft emit about 10^{15} soot particles larger than about 5 nm per kilogram of burnt fuel. Their concentration exceeds $10^6/cm^3$ near the engine exit plane. The term "soot" is used to denote all black or gray carbon-containing, nonvolatile products from incomplete combustion processes in the engine. Soot particles are composed of individual, nearly spherical particles (spherules), which have a mean radius between 10 and 30 nm. Agglomerated soot particle sizes are typically 10–100 nm in diameter. Engines emit about 0.01–0.2 g soot/kg fuel (Petzold and Döpelheuer 1998). The fleet average is near 0.04 g/kg (Petzold et al. 1999b). Graphitelike soot particles are hydrophobic. Soot particles from hydrocarbon flames are partially hydrated (Chughtai et al. 1996). The activation of soot particles that grow to droplets which then freeze is not yet fully understood (Kärcher et al. 1996). Measurements in young exhaust plumes at cruise show less soot particles outside ice particles in plumes with contrails than in plumes without contrails, indicating that the emitted soot particles participate in the formation of ice particles (Schröder et al. 1998). Also, measurements of the refractive index of particles larger than 150 nm suggest that soot enters water particles (Kuhn et al. 1998). Soot seems to be the dominant ice nucleus in the upper part of sinking contrails in the vortex regime, whereas the lower part seems to contain ice particles freshly formed mainly from ambient aerosol (Ström and Ohlsson 1998a). The number of ice particles found in aged contrails correlates with the amount of absorbing material measured and with air traffic density, indicating a relationship between ice particles in contrails and soot emissions (Ström and Ohlsson 1998b). Individual soot (and some metal) particles have been found in ice particles of aged contrails (Petzold and Schröder 1998; Twohy and Gandrud 1998; Petzold et al. 1998). Models suggest that contrails would also form without soot and sulfur emissions by activation from freezing of background particles (Jensen et al. 1998c; Kärcher et al. 1998a). However, the resulting contrails would have fewer and larger particles and hence less direct radiative impact. It is unknown whether the soot aerosol induced by air traffic in the upper troposphere causes cirrus clouds with more or less ice particles (Jensen and Toon 1997).

In addition to soot, measurements show that aircraft induce 10^{15}–4×10^{17} volatile particles larger than about 5 nm in diameter per kilogram of burnt fuel

into the young plume (Anderson et al. 1998; Kärcher et al. 1998b). This number varies strongly with the detection limit of the CN counters used. Volatile particles originate from the emitted water vapor, the sulfuric acid (formed in burning sulfur-containing fuels; mean sulfur mass content near 500ppm) and from the chemi-ions. Aerosol models (Kärcher et al. 1998b; Yu et al. 1998) show that the measured volatile particles larger than 5nm originate from chemi-ions (as measured by Arnold et al. 1998a,b) because the force between charged particles enhances coagulation (Yu and Turco 1998b). The number of volatile particles measured in plumes behind different aircraft grows with the mass fraction of sulfur in the fuel used (Schumann et al. 1996; Anderson et al. 1998; Schröder et al. 1998), indicating that part of the fuel sulfur is converted to sulfuric acid, which participates in bimolecular homogeneous or heterogeneous nucleation and condensation and enhances particle growth. For one aircraft, chemical ion mass spectrometric measurements show that 0.4–2.5% of the fuel sulfur is converted to sulfuric acid (Curtius et al. 1998). Other indirect measurements suggest much larger conversion rates (Fahey and Schumann 1999). It appears that the conversion fraction depends on the fuel-sulfur content and on the engine type (Lukachko et al. 1998; Miake-Lye et al. 1998). Recent studies suggest that some volatile material is formed from emitted hydrocarbons (Kärcher et al. 1998b).

Because of sulfuric acid formation, the number of ice particles formed in contrails increases and the mean size decreases with fuel sulfur content, though weakly. Measurements indicate that the number of ice particles increases by a factor of 2 and the mean crystal size shrinks by about 20% for fuel sulfur content increasing from 0.02 to 3g/kg (Petzold et al. 1997). Sulfuric aerosol seems to be the dominant ice-forming aerosol at temperatures far below the threshold temperature for contrail formation (Kärcher 1998), but even strong changes in fuel sulfur have only a small (<0.4K) impact on the threshold temperature (Busen and Schumann 1995; Schumann et al. 1996). However, ice crystals formed in contrails scavenge vapors and particles, creating a sulfate aerosol accumulation mode that may contribute to ice nuclei, and this source of ice nuclei is amplified with higher sulfur emissions (Yu and Turco 1998a).

It is expected that large and highly diluted sulfuric acid droplets or large-soot aerosols coated with sulfate material will have the strongest impact on cirrus ice formation (Jensen and Toon 1997). However, this relationship has not yet been determined experimentally. Also, it is not clear which air traffic parameter controls the amount of induced contrail cirrus best. Is it the fuel consumption, the number of aircraft, the number of particles emitted, or the number of ice particles formed in the plume after a few minutes? These questions need further investigations. Ice particles in young contrails (age 1–20s) are small, about 1μm in diameter. Under high ambient humidity, they grow to larger ice particles. Ice particle size spectra within and at the edge of young contrails systematically differ from each other (Petzold et al. 1997). At the edges, the relative humidity with respect to ice can be larger, causing larger ice crystals to form. Large ice particles (300μm and 2mm in diameter) have been measured in several-minutes-old plumes in very humid air (Knollenberg 1972; Heymsfield et al. 1998a), and such particles sediment quickly.

At least in some cases, the number of particles in contrails seems to be dictated mainly by the processes in the fresh plume. As a contrail spreads, the total number of particles (about 10^{11}–10^{12} ice crystals/m length of contrail) was observed to stay fairly constant (Schröder et al. 2000; Spinhirne et al. 1998). However, this observation needs to be checked further. Clearly, some particles will eventually sediment out of the contrail. In ice-supersaturated air, aircraft induce particles also by vertical air motions enhancing the relative humidity (Gierens and Ström 1998). In such cases most of the surviving ice particles originate in the wake behind the downward-traveling vortex tube generated behind aircraft. The number of ice particles per unit flight path grows with the size of the aircraft (Gierens and Ström 1998). The fraction of surviving ice crystals can be much smaller (e.g., by a factor of 200) than the number of ice particles generated in the early jet phase of the contrail (Sussmann and Gierens 1999).

Contrail ice particles may sediment and dehydrate the upper troposphere or may seed lower-level cloud formation (Knollenberg 1972). Sedimentation of ice crystals in strongly supersaturated air has been observed (Schumann 1994; Heymsfield et al. 1998a), but the significance of such precipitation is unknown.

11.3. Contrail Occurrence

Extensive contrail cirrus may form in ice-supersaturated air. Ice supersaturated regions are expected to be common in the upper troposphere but to occur rarely in the stratosphere, at least somewhat above the tropopause. In the upper troposphere, ice-saturated air masses can exist without forming clouds, as shown by the presence of persistent contrails outside cirrus clouds. Air masses become ice-supersaturated when lifted, which occurs under suitable meteorological conditions (Kästner et al. 1999). An ice-saturated air mass may reach liquid saturation when lifted 300–400 m by ambient air motions. Ice-supersaturation has been measured by high-precision frost-point hygrometers in a few localized cases (Brewer 1946; Murphy et al. 1990; Heymsfield et al. 1998b). For example, in the upper troposphere over the North Atlantic, Ovarlez et al. (1999) measured RH exceeding 150% with respect to ice saturation at –60 to –50°C ambient temperature [i.e., higher than the ice nucleation limit deduced by Heymsfield et al. (1998b)], possibly because of different nucleation properties in maritime air masses. Gierens et al. (1999b) analyzed hygrometer data taken during the MOZAIC project onboard in-service airliners of type Airbus A340 (Helten et al. 1998; Marenco et al. 1998) and found that 13.5% of all the flights occurred in air masses that are ice-supersaturated but that liquid saturation is found rarely. The MOZAIC data agreed within 5–15% of liquid saturation with in-flight frost-point measurements (Helten et al. 1999), just sufficient for this kind of analysis.

The frequency or area of coverage of Earth by contrails has been measured only in a few selected regions. At northern mid-latitudes, the contrail frequency peaks around February/March and has a minimum during July (Mazin 1996; Minnis et al. 1997). Persistent contrails were visible from surface stations over the continental United States for 12% of all observations. The observed contrail

frequency is well correlated with the fuel consumption in the same region. Hence, contrail coverage is limited by the number of aircraft flights and not by the atmospheric conditions. Contrails occur within thin cirrus in approximately 80% of the observations (Minnis et al. 1997; Sassen 1997). In situ measurements of contrails inside and outside cirrus clouds indicate that contrail growth is only weakly, if at all, affected by preexisting cirrus clouds (Schröder et al. 1998a).

Contrails often get wide and thick enough to induce radiative disturbances that are detectable in satellite data. Individual contrails have been traced in satellite pictures for up to 18 h (Minnis et al. 1998). Figure 11.2 shows the unusual example of a spiral contrail formed from a circulating military aircraft. Radiosonde data (station Schleswig of 12 UT May 22, 1998) for that region and day indicate that the contrail formed above 9 km altitude (pressure <300 hPa, temperature <–47°C) where the wind blew at more than 110 km/h from 330°.

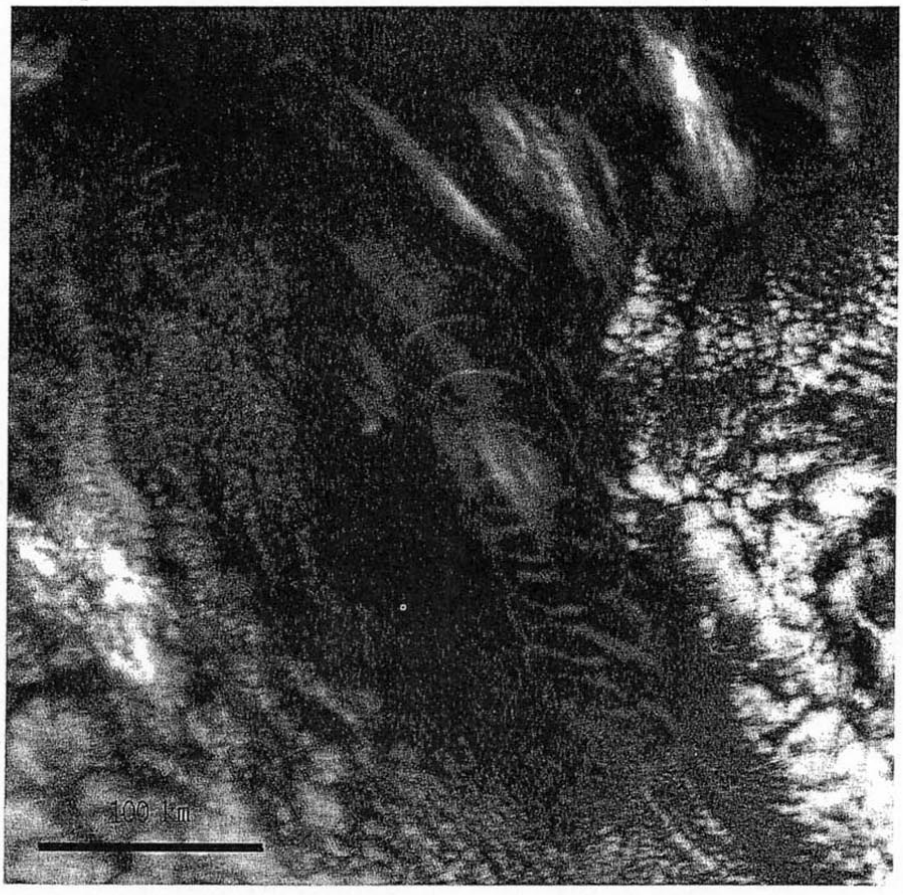

Figure 11.2. Spiral contrail observed in NOAA-14 AVHRR satellite data west of Denmark at 1236 UT, May 22, 1998, with at least eight circles of about 60 km diameter, and a shift of 195 km between the first and the eighth circle at wind speed of 110 km/h, implying a contrail length of about 1500 km and contrail age of 1.7–1.9 h. (Picture processed by H. Mannstein.)

The resultant contrail length of about 1500 km for a typical aircraft speed of 800 km/h and the shift of the circles by 195 km with the wind of known speed imply a contrail age of about 1.7–1.9 h. Line-shaped contrails are often visible in multispectral advanced very high resolution radiometer (AVHRR) satellite data. Based on AVHRR channel 4 and 5 differences (near 11 and 12 μm) and a pattern recognition algorithm to differentiate line-shaped clouds from fuzzy cirrus clouds, Mannstein et al. (1999) evaluated the contrail cover over central Europe for 666 days of the years 1995–96 using nearly all noon passages of the NOAA-14 satellite. In the annual mean, line-shaped contrails at noon cover about 0.5% of the area over central Europe. This represents a lower bound for the actual contrail cover because the algorithm cannot identify non-line-shaped contrails. During night the cover is one-third this value in this region. The day/night cover ratio depends on the local day/night traffic ratio, which is different in different regions but amounts to 2.7 in the global average (Schmitt and Brunner 1997).

Contrails persist in air masses that are cold and humid enough. From contrail observations these air masses have been estimated to cover 10–20% of the area over parts of Europe (Mannstein et al. 1999) and the United States (Carleton and Lamb 1986). This fraction is consistent with the frequency of ice-supersaturation found in MOZAIC data (Gierens et al. 1999b). Hence, as air traffic increases, persistent contrail coverage might increase up to a limit of 10–20% in these regions.

Estimates of the global cover of air masses that are cold and humid enough to carry contrails were obtained using meteorological data on temperature and humidity versus pressure altitude over the globe. Using consistently analyzed weather data of the ECMWF for this purpose together with the Schmidt-Appleman criterion and a subgrid parameterization of cirrus formation conditions, this potential contrail cover is computed to be largest in the upper troposphere (16% global mean cover; Sausen et al. 1998). The actual contrail cover is computed from the product of the potential cover and the fuel consumption rate in the same region. The product is scaled to match the observed mean contrail cover in those regions where satellite observations exist. Sausen et al. (1998) scaled their cover to the 0.5% mean cover reported by Bakan et al. (1994) for a European/Atlantic region. The computed contrail cover for linear dependence on fuel emissions of 1992 and an overall propulsion efficiency $\eta = 0.3$ reaches 5% over the eastern United States west of New York, with a zonal mean maximum of 0.6% at 50° N, and a global mean cover of 0.09%. The scaling used by Sausen et al. (1998) results in a mean cover of 1.8% in the region where Mannstein et al. (1999) report only 0.5% mean cover during day (Gierens et al. 1999a). Hence the scaling used by Sausen et al. (1998) may overestimate the actual global contrail cover.

Observations show that persistent contrails can evolve into extended cirrus that are unrecognizable as aircraft-generated clouds (Schumann and Wendling 1990; Minnis et al. 1998). Aviation-induced aerosol may also affect cirrus clouds indirectly through changes in ice-forming particles and their concentrations. Satellite data suggest that the actual impact of aircraft on cirrus cover may be larger than the computed line-shaped contrail cover. Hence, more work is needed

to determine the amount of global cover by contrails, which is about 0.1%, with an estimated uncertainty range from 0.02 to 0.2%.

The impact of aircraft-induced aerosols and contrails and related cirrus changes is expected to grow with the amount of traffic. Some long-term cirrus observations from ground and from satellites (Liepert 1997; Wylie and Menzel 1999; Boucher 1999; see Fahey and Schumann 1999) indicate increases in cirrus amounts and cirrus frequencies in regions with heavy air traffic.

Solar corona observations taken from astrophysical observatories suffer from contrails (Spannagl 1977). The radiance from the corona 40 seconds above the solar limb (0.265° from the sun's center), is typically 10^{-6}–10^{-3} times smaller than the radiance from the center of the solar disk. Even at 0.5° angular distance from the sun's center, the radiance induced by forward-scattering ice crystals in a thin cirrus cloud with optical depth 0.3 exceeds 1% of the radiance of the direct sun (Thomalla et al. 1983) and hence makes corona observations impossible. At the mountain observatory on the Wendelstein, Germany, in the northern Alps, the corona was observable on about 120 days/year from 1943 until 1961 (fig. 11.3). Thereafter, the frequency of observability declined substantially to less than 40 days/year by 1978. The number of clear-sky days and the number of solar hours at the same place did not change considerably, so the trends of the corona observations are not due to changing meteorology. Observations of the solar photosphere are less sensitive to cirrus cover and show a weaker trend than the corona observations. The personnel and the priority given to photosphere and corona observations at Wendelstein did not change until 1979. Similar trends in the number of corona days at the Pic du Midi, France, were possibly affected by changes in the personnel or priority of these observations. Data from Norikura, Japan, show no trend. The apparent decrease at Kislovodsk, Russia, until 1976 (Spannagl 1977) did not continue after 1978. The changes at the European stations appear to coincide with the onset of commercial jet traffic in the 1960s. The differences between the Japanese and European observations may be explained by different traffic densities (Spannagl 1977). Such observations are noteworthy but not conclusive. More work is needed to identify and verify or falsify any systematic relationship between air traffic and changes in cloud-related parameters.

11.4. Properties of Persistent Contrail Particles

With respect to climatic impact, short-lived contrails are unimportant because of their small degree of cover (about 10^{-6} of the Earth surface; Ponater et al. 1996). The radiative effects of contrails depend mainly on the coverage and optical depth of persistent contrails. Lidar data reveal a solar optical depth of such contrails that varies typically between 0.05 and 0.5 (Kästner et al. 1993; Jäger et al. 1998). The optical depth of contrails remains about constant during the first hour despite horizontal spreading. Occasionally, very thick contrails (order 700 m) with optical thickness greater than 1.0 are found at larger temperatures (up to –30°C; Schumann and Wendling 1990; Gayet et al. 1996). The optical depth and the radiative effects of contrails depend on the size, number, and shape of particles, and on the ice water content (IWC).

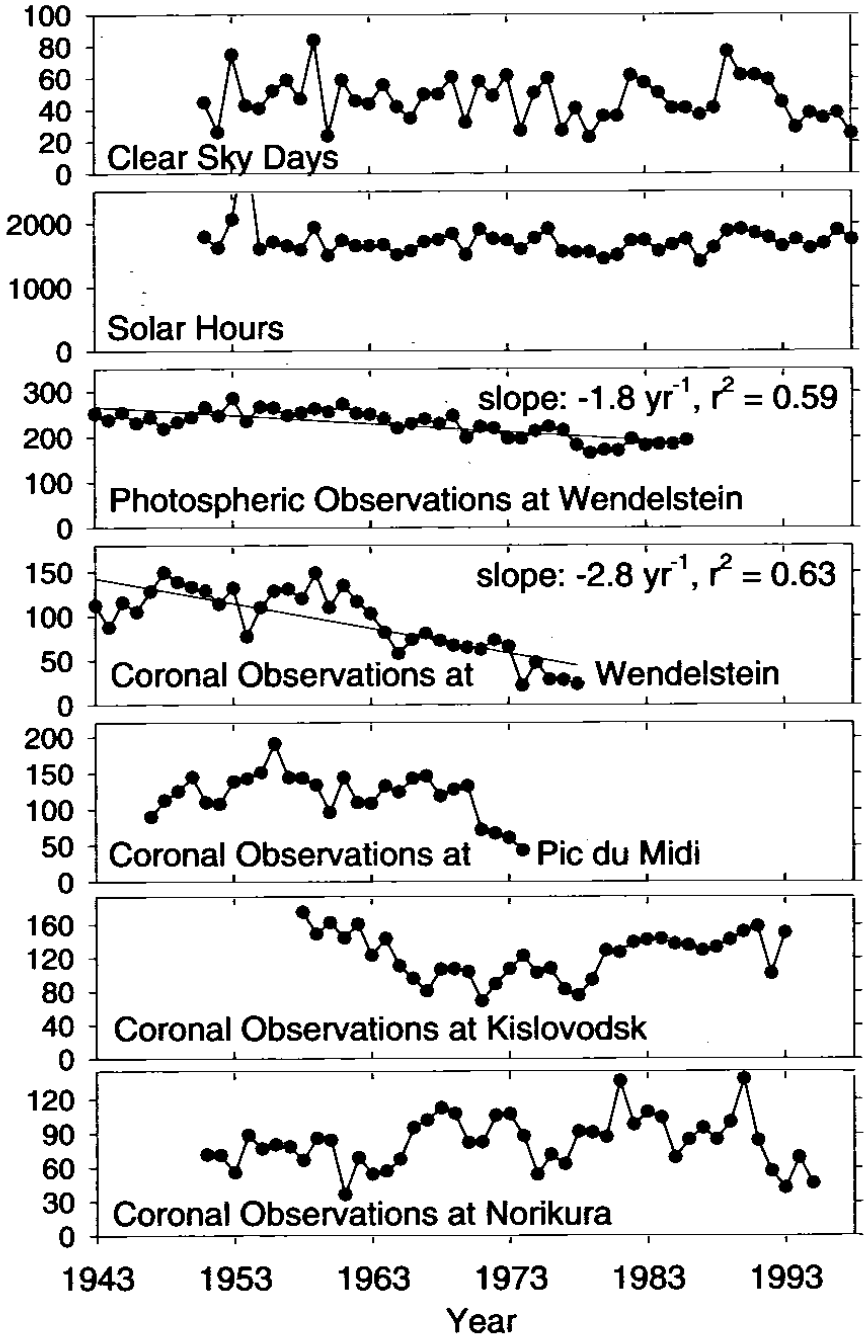

Figure 11.3. Number of clear-sky days, solar hours, days suitable for solar photospheric observations, and days suitable for solar corona observations per year at Wendelstein (1841 m above sea level, Germany, northern Alps, 12°01′ E, 47°42′ N), and number of days suitable for corona observations per year for the observatories at Pic du Midi (2861 m, Pyrennes, southern France, 8°42′ E, 42°56′ N), Kislovodsk (2130 m, Russia, 42°40′ E, 43°45′ N, east of the Black Sea), and Norikura (2876 m, Japan, 137°33′19″ E, 36°06′49″ N). Data for the period 1943–1976 are from Spannagl (1997). Data thereafter are from various sources (Deutscher Wetterdienst, München; Quarterly Bulletin on Solar Activity; yearbooks of the Wendelstein Observatory; Takashi Sakurai, Norikura Solar Observatory). Linear regressions are plotted in two panels with slopes and correlation coefficients, r^2, as given. For all other curves, correlation coefficients would be <0.2.

Contrail particle sizes increase with time in humid air. Ice crystals in young contrails are typically smaller (mean radius of 5–15 μm) than in cirrus clouds (mean radius >30–150 μm, depending on temperature; see fig. 11.4). In humid air, contrail particles may grow up to 2 mm in size (Knollenberg 1972; Strauss et al. 1997). Such large crystals are within the natural variability of cirrus particle sizes. As a consequence, old, dispersed contrails appear to have similar particle sizes as surrounding cirrus (Duda and Spinhirne 1998; Minnis et al. 1998; Schröder et al. 2000). The number of ice crystals in contrails of 10–30 min age (order 10–200/cm^3) is much larger than in cirrus clouds (Sassen 1997; Schröder et al. 2000).

Strong depolarization of lidar returns by contrails with growing particles that are a few minutes old indicate aspherical particle shapes (Freudenthaler et al. 1996; Sassen 1997). Using optical detectors and replicators, both complex ice particles (Goodman et al. 1998; Lawson et al. 1998; Liou et al. 1998; Meyers and Hallett 1998) and nearly spherical ice particles (Strauss et al. 1997; Schröder et al. 2000) were identified. Spherical particles seem to prevail at low ambient temperatures (<–55°C). At low temperatures the ice particles in the contrail core do not find enough water to grow. Hence, the particles in the core remain close to spherical, while the particles near the humid boundary of contrails may become

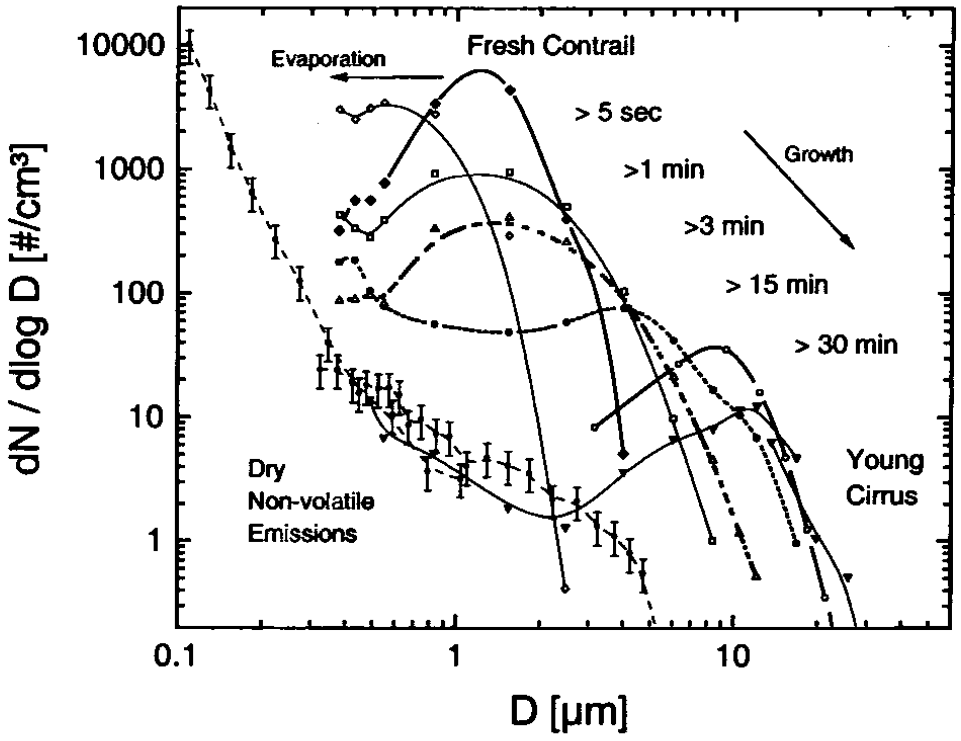

Figure 11.4. Ice particle size spectra (unit: cm^{-3}) measured with optical particle spectrometers in contrails of different ages and in young cirrus clouds and dry aerosol size spectrum (dried aerosol spectrometer PCASP probes and optical FSSP-300 spectrometer data). Adapted from Schröder et al. (2000).

large and very complex in shape, especially at high ambient temperature and humidity (Heymsfield et al. 1998a). The larger particles are of various shapes, with the largest particles being bullet rosettes (Lawson et al. 1998). No model exists yet to predict the shape of the particles forming.

The IWC of contrails depends, as for cirrus clouds, on temperature, ambient humidity, time available for water deposition, vertical motion of the ambient air, precipitation, and possibly cooling of the ice particles by radiation (Knollenberg 1972). A simple model assumed that the IWC is one half of the amount of water available for ice formation between the limit of ice nucleation and ice saturation (Meerkötter et al. 1999). The limit for ice nucleation is the RH above which nuclei grow and form ice. Heymsfield et al. (1998b) found that the critical RH for ice nucleation decreases almost linearly from water saturation (100% RH) at temperatures above –39°C to 75% RH at and below –55°C. These assumptions result in a function of IWC that depends only on temperature. As a consequence of the saturation properties of water, the IWC grows approximately exponentially with temperature (fig. 11.5). The IWC values implied by this model are a little higher than those measured in cirrus clouds (see Meerkötter et al. 1999). This is reasonable because ice particles in cirrus clouds are larger and may sediment more quickly and over longer periods than in contrails.

Figure 11.5 shows the few IWC data points that were measured within aged contrails (Gayet et al. 1996; Sassen 1997; Schröder et al. 2000), including data of the SUCCESS experiment (Heymsfield et al. 1998a). The IWC values vary between 0.7 and 18 mg/m^3. The data generally support the postulated temperature dependence of the IWC within reasonable limits. Deviations between the measured IWC values and any systematic trend are not surprising because of the difficulties in measuring IWC inside a contrail, which are due to the shortcomings of the various sensors and the representativity of such measurements in a contrail cloud, which is highly heterogeneous spatially.

The plot does not include the large IWC values reported by Knollenberg (1972). Values of up to 135 mg/m^3 at –33.5°C ambient temperature in a contrail of 30 min age exceed the amount of water vapor available for ice formation from liquid saturation at this temperature by a factor of 2. The large IWC values are hard to understand because they require that ice particles were formed in an air mass of 100% RH initially and were cooled (e.g., radiatively by about 5 K within the 30 min of contrail age). Such a cooling rate (240 K/day) can hardly be expected for the cirrus layer as a whole (Liou 1986), but large ice particles at the top of the cirrus and above lower level clouds may experience strong radiative cooling (Gierens 1994). The observations cannot be explained by rising air because the contrail was observed to descend and the data were taken 460 m below the level of contrail initialization.

If aircraft contrails cause deposition of all water vapor in excess of ice-saturation to form ice particles, the potential IWC can be computed from measured humidity values. Figure 11.5 shows the potential IWC computed from humidity data measured in the MOZAIC project (see above) and in the POLINAT project (Schumann et al. 2000). The mean values of the potential IWC values increase approximately exponentially with temperature:

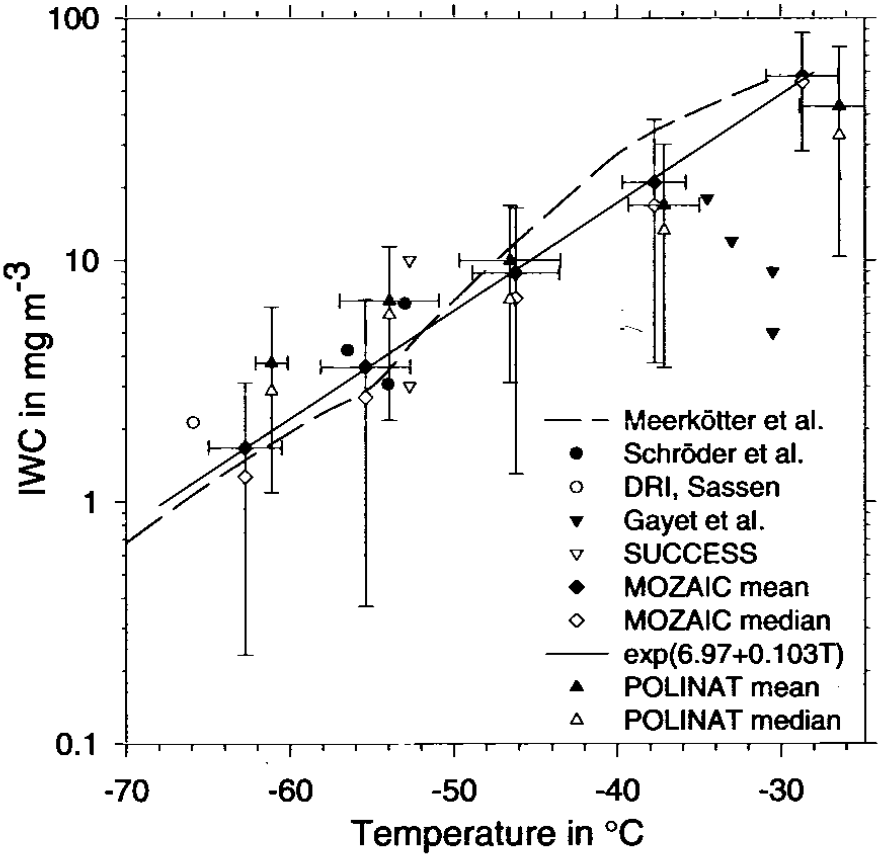

Figure 11.5. Ice water content (IWC) versus ambient temperature. The dashed curve is a proposed contrail IWC model (Meerkötter et al. 1999). The isolated symbols denote individual IWC data measured in aged contrail cirrus by Schröder et al. (2000), by the Desert Research Institute as reported by Sassen (1997), Gayet et al. (1996), and in the SUCCESS experiment between 2314 and 2322 UTC, May 12, 1996 (see Heymsfield et al. 1998). The filled and open rhombic symbols with error bars denote the mean and the median value and the standard deviations of the potential IWC and temperature deduced from humidity and temperature measurements during the MOZAIC project within the intervals from −70° to −20°C in 10°C intervals (Helten et al. 1998; Gierens et al. 1999b). The filled and open triangles with error bars denote the same from the POLINAT data (Ovarlez et al. 1999; Schumann et al. 2000). The straight full line is the linear least square fit to the logarithmic mean values of the potential IWC values from MOZAIC.

$$\mathrm{IWC}/(\mathrm{mg/m^3}) = \exp(6.97 + 0.103\mathrm{T}/^{\circ}\mathrm{C}).$$

This interpolation is close to the model proposed by Meerkötter et al. (1999) but does not show a change in trend near −39°C as would be expected if the RH of ice nucleation is 100% above and less than 100% below that temperature. Further IWC measurements in persistent contrails are needed to verify this relationship.

11.5. Radiative Forcing by Contrails

Radiative forcing by contrails is computed using one-dimensional radiative transfer models suitable for geometrically and optically thin, plane-parallel homogeneous cirrus layers in a static atmosphere (Liou 1986; Fu and Liou 1993; Fortuin et al. 1995; Strauss et al. 1997; Raschke et al. 1998). The three-dimensional effect of narrow but thin contrails seems to be small (Schulz 1998), but some measurements below thick contrails indicate smaller long-wave forcing than expected for homogeneous cloud layers (Kuhn 1970).

Cloud radiative forcing is defined as the change in net flux at some level in the atmosphere calculated in response to a perturbation in clouds for otherwise fixed atmospheric parameters. A positive net flux change represents an energy gain and hence a net heating of the Earth's system below the level considered. In most cases, contrails increase the Earth's system albedo and hence cause a negative radiative forcing in the shortwave (SW) range. Contrails have a lower temperature than the atmosphere below the contrails and hence induce a positive radiative forcing in the long-wave (LW) range. The net radiative forcing is the sum of the SW and LW contributions. In most cases, the net radiative forcing is positive at top of the atmosphere but negative at the Earth's surface, especially during daytime. The radiative forcing grows with the optical depth (or ice water path; IWP) and with the amount of contrail cover.

A parameter study of radiative forcing by contrails was reported by Meerkötter et al. (1999). The radiative forcing at the top of the atmosphere for 100% contrail cover and either spheres or randomly oriented hexagons is plotted versus time of day in figure 11.6 for a contrail with a visible optical depth of 0.5. The particle size spectrum is assumed to be the same as measured by Strauss et al. (1997) with a volume-mean particle diameter of 16.4 μm. Contrails heat most when covering a warm and bright surface. Contrails are most efficient in radiatively forcing the Earth's atmosphere in the tropics and over low-level clouds and are more efficient in summer than in winter. Contrails with smaller ice particles cause stronger heating than other cirrus with the same IWP because the albedo increases less strongly than the thermal absorption efficiency with decreasing crystal size. However, for very small crystals [i.e., for particle radius smaller than about 10 μm (depending on IWP)], a reduction in radius cools the atmosphere because the albedo increases more than the absorption efficiency. Contrails with spherical particles cause more heating than hexagonal ice particles (fig. 11.6).

At the top of the atmosphere, for a global mean contrail cover of 0.1% and an average optical depth of 0.3, contrails have been computed to cause about 0.02 W/m^2 daily mean radiative forcing in the global mean, with an estimated uncertainty factor of 4. As shown in figure 11.7c, the radiative forcing is larger regionally with maximum values of up to 0.7 W/m^2 over parts of Europe and the United States (Minnis et al. 1999). The contrail cover and, even more so, the radiative forcing is relatively large compared to fuel consumption along the narrow long-distance flight routes in the upper troposphere. For given fuel consumption, the radiative forcing is larger over Europe than over the United States. The contrail forcing appears to be larger than the radiative forcing from past carbon

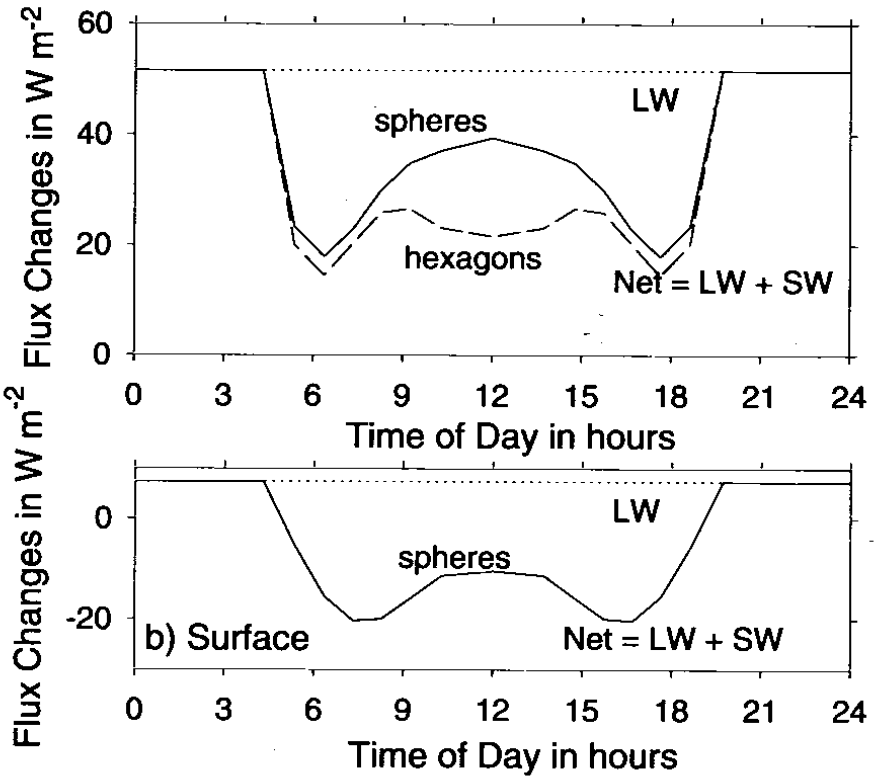

Figure 11.6. Flux changes at top of atmosphere (TOA) and at the surface versus time of day for long-wave (LW), and net (SW + LW, short-wave and long-wave) fluxes for spherical and hexagonal (shown for TOA only) particles. Adapted from Meerkötter et al. (1999).

dioxide emissions from aircraft (IPCC 1999). The biggest uncertainties of computed contrail forcing values appear to result from the not-well-known contrail cover and optical depth values and unknown impact of aircraft emissions on natural cirrus.

Contrails cause a small and slow heating of the troposphere. Strauss et al. (1997) used a one-dimensional radiative convective model to simulate the climatic conditions of a mid-European region. They found a steady-state mean temperature increase on the order of 0.05 K for a 0.5% increase in current contrail

Figure 11.7. (a) Air traffic as of 1992 in terms of vertically integrated annual mean fuel consumption [g(fuel)/m^{2}a^{-1}] above 500 hPa according to the DLR-2 data set (Schmitt and Brunner, 1997). (b) Computed contrail cover for this traffic (Sausen et al. 1998), and (c) net radiative forcing at the top of atmosphere in the daily and annual average for this contrail cover and an assumed 0.55-μm optical depth of 0.3 (Minnis et al. 1999). The contours give the percentage relative to the maximum values of 11.14 g/m^{2}a^{-1}, 5.45%, and 0.725 W/m^2, in the panels from top to bottom, respectively.

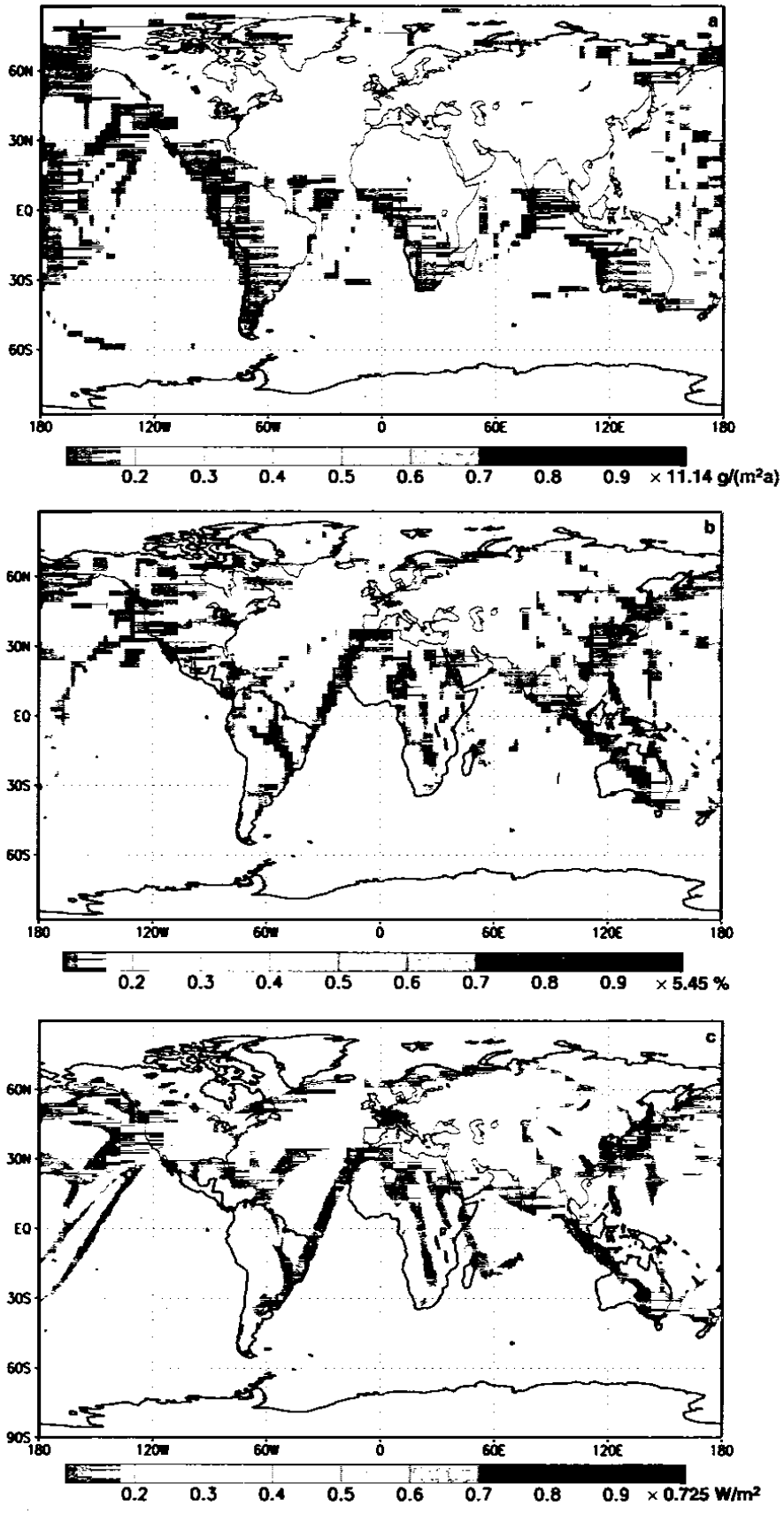
a
60N
30N
EQ
30S
60S
180
120W
60W
0
60E
120E
180
0.2 0.3 0.4 0.5 0.6 0.7 0.8 0.9 × 11.14 g/(m²a)
b
60N
30N
EQ
30S
60S
180
120W
60W
0
60E
120E
180
0.2 0.3 0.4 0.5 0.6 0.7 0.8 0.9 × 5.45 %
c
60N
30N
EQ
30S
60S
90S
180
120W
60W
0
60E
120E
180
0.2 0.3 0.4 0.5 0.6 0.7 0.8 0.9 × 0.725 W/m²

cloud cover—too small to be measurable. With a two-dimensional radiative convective model, a 1 K increase was found in surface temperature over most of the Northern Hemisphere for an additional cirrus cover of 5% (Liou et al. 1990). Using a global circulation model, the potential effects of contrails on global climate were simulated by introducing additional cirrus cover with the same optical properties as natural cirrus in air traffic regions with large fuel consumption (Ponater et al. 1996). The induced temperature change was significant for an assumed 5% additional cirrus cloud cover in the main traffic regions. These studies demonstrate the importance of contrails in climate change but do not yet provide a reliable quantitative assessment.

As illustrated in figure 11.6, contrails cool the surface during the day and heat the surface during the night and hence reduce the daily temperature amplitude. The net effect depends strongly on the daily variation of contrail cloud cover. A reduction of solar flux by 50 W/m^2, as measured by Sassen (1997), is to be expected locally in the shadow of thick contrails ($\tau > 1$). The surface LW forcing is small because of shielding of terrestrial radiation by water vapor in the atmosphere above the surface. Hence, the Earth's surface locally receives less solar energy in the shadow of contrails (Sassen 1997). This does not exclude a warming of the atmosphere-surface system driven by the net flux change at the top of the atmosphere. As shown by radiation-convection models, vertical heat exchange in the atmosphere may cause warming of the surface even when it gets less energy by radiation (Strauss et al. 1997).

Besides the forcing by line-shaped contrail cirrus, the global radiation balance may also be perturbed if there is a significant indirect effect of aircraft-induced aerosol, water vapor, and contrails on the cover and properties (particle size distribution, number density, and composition) of natural cirrus clouds. In addition, there might be other indirect cloud-related effects, such as humidity changes, precipitation, and others still to be identified. The radiative forcing from these indirect effects are unknown. Preliminary studies (Wyser and Ström 1998; Meerkötter et al. 1999) show that aircraft-induced changes in the particle size of natural cirrus clouds may cause radiative forcing comparable to the direct forcing due to additional contrail cloud cover. This requires further studies.

In the future, contrail cloudiness will increase more strongly than global aviation fuel consumption if air traffic increases mainly in the upper troposphere or if engines have larger overall efficiency, causing cooler exhaust for the same water concentration and hence contrails also at lower altitudes (an increase of the efficiency, η, from 0.3 to 0.5 reduces the threshold level of contrail formation by 700 m). The radiative forcing may increase even more when the contrail cover increases relatively more in the tropics. In a scenario for the year 2050 with a threefold increase in fuel consumption, a four- to fivefold increase in contrail cover and a sixfold increase in radiative forcing is expected (Gierens et al. 1999a). Higher cruise altitudes will increase contrail cover in the subtropics, and flying lower will increase contrail cover in polar regions (Sausen et al. 1998).

Future research should help to reduce the main uncertainties: cover and mean optical depth of contrails over the globe and indirect impact of aircraft-generated aerosols on cirrus cloudiness. For that purpose it would be interesting to know any differences between cirrus cloud properties in the Southern and

Northern hemispheres at mid-latitudes, with large differences in aerosol loading near the tropopause (Kent et al. 1998). Also, it would be important to know how long and with which areal fraction persistent contrails cover a region and impact the daily temperature range.

Acknowledgments I am grateful to important contributions that I received in preparing the material used for this review, in particular from the authors, contributors, and reviewers of the related chapter 3 of the IPCC assessment, especially David W. Fahey, Klaus Gierens, Bernd Kärcher, Ralf Meerkötter, Patrick Minnis, Robert Sausen, and O. Brian Toon. I thank Stefan Kinne for providing data from the SUCCESS experiments, Herman Smit and Alain Marenco for providing access to the MOZAIC data, Joelle Ovarlez for the frost-point temperature data measured during POLINAT, Richard Meyer and Hermann Mannstein for providing satellite data, and Franz P. Schröder, David R. Doelling, and Klaus Gierens for providing materials and figures prior to publication. I thank Otto Bärnbantner, Heinz Barwig, Guido Kugelmann, Jean-Louis Leroy, Christian Spannagl, Takashi Sakurai, and Peter Wendling for help in collecting and understanding the data shown in figure 11.3. Finally, I thank David K. Lynch for inviting me to contribute to this book.

References

Anderson, B.E., W.R. Cofer, D.R. Bagwell, J.W. Barrick, C.H. Hudgins, and K.E. Brunke, 1998. Airborne observations of aircraft aerosol emissions I: Total nonvolatile particle emission indices. *Geophys. Res. Lett.*, **25**, 1689–1692.

Appleman, H., 1953. The formation of exhaust contrails by jet aircraft. *Bull. Amer. Meteor. Soc.*, **34**, 14–20.

Arnold, F., T. Stilp, R. Busen, and U. Schumann, 1998a. Jet engine exhaust chemi-ion measurements: Implications for gaseous SO_3 and H_2SO_4. *Atmos. Environ.*, **32**, 3073–3077.

Arnold, F., K.-H. Wohlfrom, M.W. Klemm, J. Schneider, K. Gollinger, U. Schumann, and R. Busen, 1998b. First gaseousion composition measurements in the exhaust plume of a jet aircraft in flight: Implications for gaseous sulfuric acid, aerosols, and chemiions. *Geophys. Res. Lett.*, **25**, 2137–2140.

Bakan, S., M. Betancor, V. Gayler, and H. Grassl, 1994. Contrail frequency over Europe from NOAA-satellite images. *Ann. Geophys.*, **12**, 962–968.

Boucher, O., 1999. Influence of air traffic on cirrus occurrence. *Nature*, **397**, 30–31.

Brewer, A.W., 1946. Condensation trails. *Weather*, **1**, 34–40.

Busen, R., and U. Schumann, 1995. Visible contrail formation from fuels with different sulfur contents. *Geophys. Res. Lett.*, **22**, 1357–1360.

Carleton, A.M., and P.J. Lamb, 1986. Jet contrails and cirrus clouds: A feasibility study employing high-resolution satellite imagery. *Bull. Amer. Meteor. Soc.*, **67**, 301–309.

Chughtai, A.R., M.E. Brooks, and D.M. Smith, 1996. Hydration of black carbon. *J. Geophys. Res.*, **101**, 19505–19514.

Coleman, R.F., 1996. A new formulation for the critical temperature for contrail formation. *J. Appl. Meteor.*, **35**, 2270–2282.

Curtius, J., B. Sierau, F. Arnold, R. Baumann, R. Busen, P. Schulte, and U. Schumann, 1998. First direct sulfuric acid detection in the exhaust plume of a jet aircraft in flight. *Geophys. Res. Lett.*, **25**, 923–926.

Duda, D.P., and J.D. Spinhirne, 1996. Split-window retrieval of particle size and optical depth in contrails located above horizontally inhomogeneous ice clouds. *Geophys. Res. Lett.*, **23**, 3711–3714.

Fahey, D.W., and U. Schumann, 1999. Aviation-Produced Aerosols and Cloudiness. In *Aviation and the Global Atmosphere, A Special Report of the Intergovernmental Panel on Climate Change* (J.E. Penner, D.H. Lister, D.J. Griggs, D.J. Dokken, and M. McFarland, eds.), Cambridge Univ. Press, Cambridge, UK, pp. 65–120.

Ferris, P.D., 1996. The formation and forecasting of condensation trails behind modern aircraft. *Meteorol. Appl.*, **3**, 301–306.

Fortuin, J.P.F., R. van Dorland, W.M.F. Wauben, and H. Kelder, 1995. Greenhouse effects of aircraft emissions as calculated by a radiative transfer model. *Ann. Geophys.*, **13**, 413–418.

Freudenthaler, V., F. Homburg, and H. Jäger, 1995. Contrail observations by ground-based scanning lidar: Cross-sectional growth. *Geophys. Res. Lett.*, **22**, 3501–3504.

Freudenthaler, V., F. Homburg, and H. Jäger, 1996. Optical parameters of contrails from lidar measurements: Linear depolarization. *Geophys. Res. Lett.*, **23**, 3715–3718.

Fu, Q., and K.N. Liou, 1993. Parameterization of the radiative properties of cirrus clouds. *J. Atmos. Sci.*, **50**, 2008–2025.

Gayet, J.-F., G. Febvre, G. Brogniez, H. Chepfer, W. Renger, and P. Wendling, 1996. Microphysical and optical properties of cirrus and contrails: Cloud field study on 13 October 1989. *J. Atmos. Sci.*, **53**, 126–138.

Gerz, T., T. Dürbeck, and P. Konopka, 1998. Transport and effective diffusion of aircraft emissions. *J. Geophys. Res.*, **103**, 25905–25913.

Gierens, K., 1994. The influence of radiation on the diffusional growth of ice crystals. *Beitr. Phys. Atmos.*, **67**, 181–193.

Gierens, K., 1996. Numerical simulations of persistent contrails. *J. Atmos. Sci.*, **53**, 3333–3348.

Gierens, K., and E. Jensen, 1998. A numerical study of the contrail-to-cirrus transition. *Geophys. Res. Lett.*, **25**, 4341–4344.

Gierens, K., R. Sausen, and U. Schumann, 1999a. A diagnostic study of the global coverage by contrails. Part II: Future air traffic scenarios. *Theor. Appl. Climatol.*, **63**, 1–9.

Gierens, K., U. Schumann, M. Helten, H. Smit, and A. Marenco, 1999b. A distribution law for relative humidity in the upper troposphere and lower stratosphere derived from three years of MOZAIC measurements. *Ann. Geophys.*, **17**, 1218–1226.

Gierens, K.M., and J. Ström, 1998. A numerical study of aircraft wake induced cloud formation. *J. Atmos. Sci.*, **55**, 3253–3263.

Goodman, J., R.F. Pueschel, E.J. Jensen, S. Verma, G.V. Ferry, S.D. Howard, S.A. Kinne, and D. Baumgardner, 1998. Shape and size of contrail ice particles. *Geophys. Res. Lett.*, **25**, 1327–1330.

Hagen, D.E., P. Whitefield, J. Paladino, M. Trueblood, and H. Lilenfeld, 1998. Particulate sizing and emission indices for a jet engine exhaust sampled at cruise. *Geophys. Res. Lett.*, **25**, 1681–1684.

Hagen, D.E., P.D. Whitefield, and H. Schlager, 1996. Particulate emissions in the exhaust plume from commercial jet aircraft under cruise conditions. *J. Geophys. Res.*, **101**, 19551–19557.

Helten, M., H.G.J. Smit, D. Kley, J. Ovarlez, H. Schlager, R. Baumann, U. Schumann, P. Nedelec, and A. Marenco, 1990. In-flight intercomparison of MOZAIC and POLINAT water vapor measurements, 1999. *J. Geophys. Res.*, **104**, 26087–26096.

Helten, M., H.G.J. Smit, W. Sträter, D. Kley, P. Nedelec, M. Zöger, and R. Busen, 1998. Calibration and performance of automatic compact instrumentation for the mea-

surement of relative humidity from passenger aircraft. *J. Geophys. Res.*, **103**, 25643–25652.

Heymsfield, A.J., R.P. Lawson, and G.W. Sachse, 1998a. Growth of ice crystals in a precipitating contrail. *Geophys. Res. Lett.*, **25**, 1335–1338.

Heymsfield, A.J., L.M. Miloshevich, C. Twohy, G. Sachse, and S. Oltmans, 1998b. Upper tropospheric relative humidity observations and implications for cirrus ice nucleation. *Geophys. Res. Lett.*, **25**, 1343–1346.

Intergovernmental Panel on Climate Change (IPCC), 1999. *Aviation and the Global Atmosphere* (J.E. Penner, D.H. Lister, D.J. Griggs, D.J. Dokken, and M. McFarland, eds.), Cambridge Univ. Press, Cambridge, UK, p. 373.

Jäger, H., V. Freudenthaler, and F. Homburg, 1998. Remote sensing of optical depth of aerosols and cloud cover related to air traffic. *Atmos. Environ.*, **32**, 3123–3127.

Jensen, E.J., A.S. Ackerman, D.E. Stevens, O.B. Toon, and P. Minnis, 1998a. Spreading and growth of contrails in a sheared environment. *J. Geophys. Res.*, **103**, 31557–31568.

Jensen, E.J., and O.B. Toon, 1997. The potential impact of soot particles from aircraft exhaust on cirrus clouds. *Geophys. Res. Lett.*, **24**, 249–252.

Jensen, E.J., O.B. Toon, S. Kinne, G.W. Sachse, B.E. Anderson, K.R. Chan, C.H. Twohy, B. Gandrud, A. Heymsfield, and R.C. Miake-Lye, 1998b. Environmental conditions required for contrail formation and persistence. *J. Geophys. Res.*, **103**, 3929–3936.

Jensen, E.J., O.B. Toon, R.F. Pueschel, J. Goodman, G.W. Sachse, B.E. Anderson, K.R. Chan, D. Baumgardner, and R.C. Miake-Lye, 1998c. Ice crystal nucleation and growth in contrails forming at low ambient temperatures. *Geophys. Res. Lett.*, **25**, 1371–1374.

Kärcher, B., 1996. Aircraft-generated aerosols and visible contrails. *Geophys. Res. Lett.*, **23**, 1933–1936.

Kärcher, B., 1998. Physicochemistry of aircraft-generated liquid aerosols, soot, and ice particles, 1, Model description. *J. Geophys. Res.*, **103**, 17111–17128.

Kärcher, B., R. Busen, A. Petzold, F.P. Schröder, U. Schumann, and E.J. Jensen, 1998a. Physicochemistry of aircraft-generated liquid aerosols, soot, and ice particles, 2, Comparison with observations and sensitivity studies. *J. Geophys. Res.*, **103**, 17129–17147.

Kärcher, B., Th. Peter, U.M. Biermann, and U. Schumann, 1996. The initial composition of jet condensation trails. *J. Atmos. Sci.*, **53**, 3066–3083.

Kärcher, B., F. Yu, F.P. Schröder, and R.P. Turco, 1998b. Ultrafine aerosol particles in aircraft plumes: Analysis of growth mechanisms. *Geophys. Res. Lett.*, **25**, 2793–2796.

Kästner, M., K.T. Kriebel, R. Meerkötter, W. Renger, G.H. Ruppersberg, and P. Wendling, 1993. Comparison of cirrus height and optical depth derived from satellite and aircraft measurements. *Mon. Wea. Rev.*, **121**, 2708–2717.

Kästner, M., R. Meyer, and P. Wendling, 1999. Influence of weather conditions on the distribution of persistent contrails. *Meteorol. Appl.*, **6**, 261–271.

Kent, G.S., C.R. Trepte, and P.L. Lucker, 1998. Long-term stratospheric aerosol and gas experiment I and II measurements of upper tropospheric aerosol extinction. *J. Geophys. Res.*, **103**, 28863–28874.

Knollenberg, R.G., 1972. Measurements of the growth of ice budget in a persisting contrail. *J. Atmos. Sci.*, **29**, 1367–1374.

Konopka, P., U. Schumann, H. Schlager, D.E. Hagen, P.D. Whitefield, and J. Ovarlez, 1997. Particulate emissions of commercial jet aircraft under cruise conditions. Institut für Physik der Atmosphäre, report no. 93, Deutsches Zentrum für Luft- und Raumfahrt, DLR Oberpfaffenhofen, Germany.

Kuhn, P.M., 1970. Airborne observations of contrail effects on the thermal radiation budget. *J. Atmos. Sci.*, **27**, 937–942.

Kuhn, M., A. Petzold, D. Baumgardner, and F.P. Schröder, 1998. Particle composition of a young condensation trail and of upper tropospheric aerosol. *Geophys. Res. Lett.*, **25**, 2679–2682.

Lawson, R.P., A.J. Heymsfield, S.M. Aulenbach, and T.L. Jensen, 1998. Shapes, sizes and light scattering properties of ice crystals in cirrus and a persistent contrail during SUCCESS. *Geophys. Res. Lett.*, **25**, 1331–1334.

Lewellen, D.C., and W.S. Lewellen, 1996. Large eddy simulations of the vortex-pair breakup in aircraft wakes. *AIAA Journal*, **34**, 2337–2345.

Liepert, B.G., 1997. Recent changes in solar radiation under cloudy conditions. *Int. J. Climat.*, **17**, 1581–1593.

Liou, K., 1986. Influence of cirrus clouds on weather and climate processes: A global perspective. *Mon. Wea. Rev.*, **114**, 1167–1199.

Liou, K.-N., S.C. Ou, and G. Koenig, 1990. An investigation of the climatic effect of contrail cirrus. In *Air Traffic and the Environment: Background, Tendencies, and Potential Global Atmospheric Effects* (U. Schumann, ed.). Springer-Verlag, Berlin, pp. 154–169.

Liou, K.N., P. Yang, Y. Takano, K. Sassen, T. Charlock, and W. Arnott, 1998. On the radiative properties of contrail cirrus. *Geophys. Res. Lett.*, **25**, 1161–1164.

Lukachko, S.P., I.A. Waitz, R.C. Miake-Lye, R.C. Brown, and M.R. Anderson, 1998. Production of sulfate aerosol precursors in the turbine and exhaust nozzle of an aircraft engine. *J. Geophys. Res.*, **103**, 16159–16174.

Mannstein, H., R. Meyer, and P. Wendling, 1999. Operational detection of contrails from NOAA-AVHRR-data. *Int. J. Remote Sensing*, **20**, 1641–1660.

Marenco, A., V. Thouret, P. Nédélec, H. Smit, M. Helten, D. Kley, F. Karcher, P. Simon, K. Law, J. Pyle, G. Poschmann, R. von Wrede, C. Hume, and T. Cook, 1998. Measurement of ozone and water vapor by Airbus in-service aircraft: The MOZAIC airborne program, an overview. *J. Geophys. Res.*, **103**, 25631–25642.

Mazin, I.P., 1996. Aircraft condensation trails. *Iz. Atmos. Oceanic Phys.*, **32**, 1–13.

Meerkötter, R., U. Schumann, D.R. Doelling, P. Minnis, T. Nakajima, and Y. Tsushima, 1999. Radiative forcing by contrails. *Ann. Geophys*, **17**, 1080–1094.

Meyers, M., and J. Hallett, 1998. Ice crystal morphology in aircraft contrails and cirrus. In *Proceedings of the Conference on Cloud Physics*, August 17–21, 1998, Everett, WA. American Meteorological Society, Boston, MA, p. 4.

Miake-Lye, R.C., B.E. Anderson, W.R. Cofer, H.A. Wallio, G.D. Nowicki, J.O. Ballenthin, D.E. Hunton, W.B. Knighton, T.M. Miller, J.V. Seeley, and A.A. Viggiano, 1998. SO_x oxidation and volatile aerosol in aircraft exhaust plumes depend on fuel sulfur content. *Geophys. Res. Lett.*, **25**, 1677–1680.

Miake-Lye, R.C., M. Martinez-Sanchez, R.C. Brown, and C.E. Kolb, 1993. Plume and wake dynamics, mixing and chemistry behind an HSCT aircraft. *J. Aircraft*, **30**, 467–479.

Minnis, P., J.K. Ayers, and S.P. Weaver, 1997. Surface-based observations of contrail occurrence frequency over the U.S., April 1993–April 1994. NASA Reference publ. 1404. National Aeronautics and Space Administration, Washington, DC.

Minnis, P., U. Schumann, D.R. Doelling, K.M. Gierens, and D.W. Fahey, 1999. Global distribution of contrail radiative forcing. *Geophys. Res. Lett.*, **26**, 1853–1856.

Minnis, P., D.F. Young, D.P. Garber, L. Nguyen, W.L. Smith, Jr., and R. Palikonda, 1998. Transformation of contrails into cirrus during SUCCESS. *Geophys. Res. Lett.*, **25**, 1157–1160.

Murphy, D.M., K.K. Kelly, A.F. Tuck, and M.H. Proffitt, 1990. Ice saturation at the tropopause observed from the ER-2 aircraft. *Geophys. Res. Lett.*, **17**, 353–356.

Ovarlez, J., H. Ovarlez, R.-M. Philippe, and J. Capus, 1999. Water vapor measurements during POLINAT 2 experiment. In *Final POLINAT-2 Report* (U. Schumann, ed.). Air Pollution Research Report EUR 18877 EN, Luxembourg, Brussels, pp. 111–120.

Petzold, A., R. Busen, F.P. Schröder, R. Baumann, M. Kuhn, J. Ström, D.E. Hagen, P.D. Whitefield, D. Baumgardner, F. Arnold, S. Borrmann, and U. Schumann, 1997. Near field measurements on contrail properties from fuels with different sulfur content. *J. Geophys. Res.*, **102**, 29867–29881.

Petzold, A., and A. Döpelheuer, 1998. Reexamination of black carbon mass emission indices of a jet engine. *Aerosol. Sci. and Techn.*, **29**, 355–356.

Petzold, A., and F.P. Schröder, 1998. Jet engine exhaust aerosol characterization. *Aerosol Sci. Tech.*, **28**, 62–76.

Petzold, A., J. Ström, S. Ohlsson, and F.P. Schröder, 1998. Elemental composition and morphology of ice-crystal residual particles in cirrus clouds and contrails. *Atmos. Res.*, **49**, 21–34.

Petzold, A., J. Ström, F.P. Schröder, and B. Kärcher, 1999a. Carbonaceous aerosol in jet engine exhaust: Emission characteristics and implications for heterogeneous chemistry. *Atmos. Environ*, **33**, 2689–2698.

Petzold, A., A. Döpelheuer, C.A. Brock, and F.P. Schröder, 1999b. In situ observations and model calculations of black carbon emission by aircraft at cruise altitude. *J. Geophys. Res.*, **104**, 22171–22181.

Ponater, M., S. Brinkop, R. Sausen, and U. Schumann, 1996. Simulating the global atmospheric response to aircraft water vapour emissions and contrails: A first approach using a GCM. *Ann. Geophys.*, **14**, 941–960.

Pueschel, R.F., S. Verma, G.V. Ferry, S.D. Howard, S. Vay, S.A. Kinne, J. Goodman, and A.W. Strawa, 1998. Sulfuric acid and soot particle formation in aircraft exhaust. *Geophys. Res. Lett.*, **25**, 1685–1588.

Raschke, E., P. Flamant, Y. Fouquart, P. Hignett, H. Isaka, P.R. Jonas, H. Sundquist, and P. Wendling, 1998. Cloud-radiation studies during the European Cloud and Radiation Experiment (EUCREX). *Surveys Geophys.*, **19**, 89–138.

Sassen, K., 1997. Contrail-cirrus and their potential for regional climate change. *Bull. Amer. Meteor. Soc.*, **78**, 1885–1903.

Sassen, K., and C.-Y. Hsueh, 1998. Contrail properties derived from high-resolution polarization lidar studies during SUCCESS. *Geophys. Res. Lett.*, **25**, 1165–1168.

Sausen, R., K. Gierens, M. Ponater, and U. Schumann, 1998. A diagnostic study of the global distribution of contrails: Part I: Present day climate. *Theor. Appl. Climatol.*, **61**, 127–141.

Schmidt, E., 1941. Die Entstehung von Eisnebel aus den Auspuffgasen von Flugmotoren. In *Schriften der Deutschen Akademie der Luftfahrtforschung*. Verlag R. Oldenbourg, München, Heft 44, pp. 1–15.

Schmitt, A., and B. Brunner, 1997. Emissions from aviation and their development over time. In DLR-Mitteilung 97-04, Deutsches Zentrum für Luft- und Raumfahrt, Köln, Germany, pp. 37–52.

Schrader, M.L., 1997. Calculations of aircraft contrail formation critical temperatures. *J. Appl. Meteor.*, **36**, 1725–1728.

Schröder, F., B. Kärcher, C. Duroure, J. Strom, A. Petzold, J.-F. Gayet, B. Strauss, P. Wendling, and A. Thomas, 2000. On the transition of contrails into cirrus clouds. *J. Atmos. Sci.*, **57**, 464–480.

Schröder, F.P., B. Kärcher, A. Petzold, R. Baumann, R. Busen, C. Hoell, and U. Schumann, 1998. Ultrafine aerosol particles in aircraft plumes: *In situ* observations. *Geophys. Res. Lett.*, **25**, 2789–2792.

Schulz, J., 1998. On the effect of cloud inhomogeneity on area-averaged radiative properties of contrails. *Geophys. Res. Lett.*, **25**, 1427–1430.

Schumann, U., 1994. On the effect of emissions from aircraft engines on the state of the atmosphere. *Ann. Geophys.*, **12**, 365–384.

Schumann, U., 1996a. On conditions for contrail formation from aircraft exhausts. *Meteor. Z.*, **5**, 4–23.

Schumann, U., 1996b. Particle formation in jet aircraft exhausts and contrails for different sulfur containing fuels. In *Nucleation and Atmospheric Aerosols 1996* (M. Kulmala and P.E. Wagner, eds.). Pergamon Press, Oxford, pp. 296–299.

Schumann, U., H. Schlager, F. Arnold, R. Baumann, P. Haschberger, and O. Klemm, 1998. Dilution of aircraft exhaust plumes at cruise altitudes. *Atmos. Environ.*, **32**, 3097–3103.

Schumann, U., H. Schlager, F. Arnold, J. Ovarlez, H. Kelder, Ø. Hov, G. Hayman, I.S.A. Isaksen, J. Staehelin, and P.D. Whitefield, 2000. Pollution from aircraft emissions in the North Atlantic flight corridor: Overview on the POLINAT projects. *J. Geophys. Res.*, **105**, 3605–3631.

Schumann, U., J. Ström, R. Busen, R. Baumann, K. Gierens, M. Krautstrunk, F.P. Schröder, and J. Stingl, 1996. *In situ* observations of particles in jet aircraft exhausts and contrails for different sulfur containing fuels. *J. Geophys. Res.*, **101**, 6853–6869.

Schumann, U., and P. Wendling, 1990. Determination of contrails from satellite data and observational results. In *Air Traffic and the Environment—Background, Tendencies, and Potential Global Atmospheric Effects* (U. Schumann, ed.). Springer-Verlag, Heidelberg, pp. 138–153.

Spannagl, C., 1977. Intensitätsmessungen der Sonnenkorona in der Linie $\lambda = 530.3\,\text{nm}$. Dissertation. Fachbereich Physik, Ludwig-Maximilians-Universität München.

Spinhirne, J.D., W.D. Hart, and D.P. Duda, 1998. Evolution of the morphology and microphysics of contrail cirrus from airborne remote sensing. *Geophys. Res. Lett.*, **25**, 1153–1156.

Strauss, B., R. Meerkötter, B. Wissinger, P. Wendling, and M. Hess, 1997. On the regional climatic impact of contrails: Microphysical and radiative properties of contrails and natural cirrus clouds. *Ann. Geophys.*, **15**, 1457–1467.

Ström, J., and S. Ohlsson, 1998a. Real-time measurement of absorbing material in contrail ice using a counterflow virtual impactor. *J. Geophys. Res.*, **103**, 8737–8741.

Ström, J., and S. Ohlsson, 1998b. *In situ* measurements of enhanced crystal number densities in cirrus clouds caused by aircraft exhaust. *J. Geophys. Res.*, **103**, 11355–11361.

Sussmann, R., 1999. Vertical dispersion of an aircraft wake: Aerosol-lidar analysis of entrainment and detrainment in the vortex regime. *J. Geophys. Res.*, **104**, 2117–2129.

Sussmann, R., and K. Gierens, 1999. Lidar and numerical studies on the different evolution of vortex pair and secondary wake in young contrails. *J. Geophys. Res.*, **104**, 2131–2142.

Thomalla, E., P. Köpke, H. Müller, and H. Quenzel, 1983. Circumsolar radiation for various atmospheric conditions. *Solar Energy*, **30**, 575–587.

Twohy, C.H., and B.W. Gandrud, 1998. Electron microscope analysis of residual particles from aircraft contrails. *Geophys. Res. Lett.*, **25**, 1359–1362.

Wylie, D.P., and W.P. Menzel, 1999. Eight years of global high cloud statistics using HIRS. *J. Climate*, **12**, 170–184.

Wyser, K., and J. Ström, 1998. A possible change in cloud radiative forcing due to aircraft exhaust. *Geophys. Res. Lett.*, **25**, 1673–1676.

Yu, F., and R.P. Turco, 1998a. Contrail formation and impacts on aerosol properties in aircraft plumes: Effects of fuel sulfur content. *Geophys. Res. Lett.*, **25**, 313–316.

Yu, F., and R.P. Turco, 1998b. The formation and evolution of aerosols in stratospheric aircraft plumes: Numerical simulations and comparisons with observations. *J. Geophys. Res.*, **103**, 25915–25934.

Yu, F., R.P. Turco, B. Kärcher, and F.P. Schröder, 1998. On the mechanisms controlling the formation and properties of volatile particles in aircraft wakes. *Geophys. Res. Lett.*, **25**, 3839–3842.